Journal of Thermal Analysis and Calorimetry (2023) 148:6761–6777
https://doi.org/10.1007/s10973-023-12198-x

# Characterizing the thermal phase behaviour of fipronil polymorphs

**Dennis Simbarashe Moyo[1,2] · Elizabet Margaretha van der Merwe[1] · Melanie Rademeyer[1] · Frederick Pieter Malan[1] · Maria T. Atanasova[3] · António Benjamim Mapossa[2,3] · Walter Wilhelm Focke[2,3]**

Received: 7 December 2022 / Accepted: 16 April 2023 / Published online: 9 May 2023


**Abstract**
This manuscript reports the investigation of the polymorphic behaviour of fipronil using a systematic comparison of the thermochemical and structural properties of different crystal forms obtained in this study as well as those previously reported in literature. The analytical techniques employed include DSC, TGA, PXRD, SCXRD and hot stage microscopy. DSC proved particularly useful because it made it possible to differentiate between the two different crystal forms found in the as-received neat fipronil. The DSC scans revealed the presence of two polymorphs which had melting endotherms with peak maxima at *ca*. 196 °C and 205 °C, respectively. These polymorphs were successfully separated via sublimation and resulted in a metastable, lower melting polymorph in the sublimate and a thermodynamically stable, higher melting form in the sublimation residue. Clear evidence for the instability of the lower melting polymorph was found when the endotherms were examined under a range of heating rates. The proportion of the metastable form appeared to increase as the rate was increased, indicating that the metastable form underwent a solid–solid phase transition to the stable form at low heating rates. Recrystallization of fipronil from different solvents yielded five different forms. TGA curves revealed that all forms, except the acetone-derived one, were solvate pseudo-polymorphs that showed solvent loss between 60 and 100 °C. The acetone-derived sample was a hemihydrate that only started to show mass loss at 120 °C. SCXRD studies revealed that three of the five forms have similar structural characteristics, while the other two forms differ notably from each other and the rest of the structures. Despite these structural differences, all five forms exhibit near-identical intra- and intermolecular hydrogen bond networks.

**Keywords** Fipronil · Polymorph · Solvate · TGA · DSC · XRD

## Introduction

Polymorphism is a phenomenon where a given chemical compound exists in at least two different crystalline arrangements in the solid state [1]. The crystal structures may differ from one another with respect to their physical properties, but they lead to identical liquid and vapour states [2, 3]. Solvates are crystalline solids that contain molecules of a solvent inside their crystal assembly, either stoichiometrically or non-stoichiometrically [4]. In pseudo-polymorphic solvates, the solvent guest molecule occupies structural voids in a crystal without being tightly associated with the lattice [1, 4]. Concomitant polymorphism corresponds to the situation where two or more different polymorphs form simultaneously during crystallization [3]. Polymorphism is a subject of great interest because the differences in structure result in the variation of properties such as melting and sublimation temperatures, heat capacity, density, solubility, dissolution rates, pharmacological activity, particle size, and stability [4, 5]. In fact, the physical properties of an active ingredient, e.g. fipronil, affect the formulation strategy of a product and its ultimate efficacy [6, 7].

This work aimed to investigate polymorphism in fipronil, also known as 5-amino-1-[2,6-dichloro-4-(trifluoromethyl) phenyl]-4-[(trifluoromethyl)sulfinyl]-1H-pyrazole-3-carbonitrile. Fipronil (Fig. 1) is a broad spectrum, low-application-rate insecticide that belongs to the class of compounds

✉ Dennis Simbarashe Moyo
dennis.moyo@up.ac.za

[1] Department of Chemistry, University of Pretoria, Lynnwood Road, Pretoria, South Africa

[2] UP Institute for Sustainable Malaria Control & MRC Collaborating Centre for Malaria Research, University of Pretoria, Private Bag X20, Hatfield, Pretoria 0028, South Africa

[3] Institute of Applied Materials, Department of Chemical Engineering, University of Pretoria, Lynnwood Road, Pretoria, South Africa

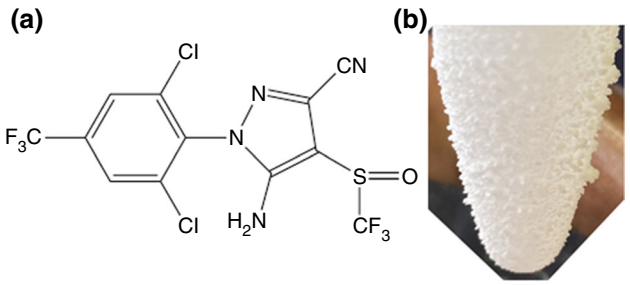


**Fig. 1** **a** The chemical structure of fipronil, and **b** the appearance of fipronil crystal deposits collected on the cold finger of the sublimation apparatus

known as phenylpyrazoles [8–11]. This systemic neurotoxin is widely used for controlling pest organisms of animals and crops, e.g. fleas, weevils, ants, ticks, rootworms, mosquitoes, and termites [12]. Fipronil and its major metabolite, fipronil sulfone, kill insects by non-competitively binding to the γ-aminobutyric acid (GABA) receptor causing the blocking of the channels involved in the transmission of neural signals [13, 14]. Its distinctive mode of action presents a potent alternative for controlling insects that have developed resistance to conventional insecticides such as pyrethroids, carbamates, organophosphates and organochlorines [10, 15].

According to patents [6, 7, 16–19] and open literature [20], fipronil exists in several different polymorphic/pseudo-polymorphic forms. These forms were characterized by powder X-ray diffraction (PXRD), infrared spectroscopy (IR), differential scanning calorimetry (DSC) and thermogravimetric analysis (TGA). Saxell et al. reported four polymorphs of fipronil which they named crystalline modifications CM-I [17], CM-II [18], CM-IV [16] and CM-V [7]. Crystalline modifications CM-I and CM-V were identified to be the thermodynamically stable forms with melting temperatures corresponding to 196 °C and 203 °C, respectively. The crystalline modifications CM-II and CM-IV were identified to be solvates of their corresponding co-crystallized solvents. The removal of the co-crystallized solvent in crystalline modifications CM-II and CM-IV resulted in endothermic phase transformations leading to crystalline modifications CM-I and CM-V and/or mixtures of them. Table 1 summarises some of the characteristics of the fipronil modifications reported by Saxell et al. [7, 16–18].

Zamir [6, 19] reported five polymorphs of fipronil which were named Form F-I, F-II, F-III, FS-T and FS-M. The DSC curve of Form F-I featured a single dominant endotherm ascribed to melting centred at 202.5 °C while the curve for Form F-II featured a second endotherm at *ca*. 195 °C. The melting points reported for Form F-I and F-II are similar to those reported by Saxell et al. for crystalline modification CM-V [7] and CM-I [17], respectively. Fortunately, both patent data sets reported PXRD patterns for the different polymorphs which they identified. Perusal of these diffractograms indicated a correspondence between F-I and CM-V as well as between F-II and CM-I. Crystal modifications CM-IV and Form F-III do not have corresponding polymorphs listed in the two separate sets of patents. FS-T and FS-M were considered hemisolvates. They contained co-crystallized toluene and methyl isobutyl ketone (MIBK), respectively. The removal of the co-crystallized toluene from FS-T by heating the sample in a DSC resulted in an endothermic phase transformation of FS-T to Form F-III at *ca*. 110 °C. Upon heating, Form F-III underwent an exothermic transformation to Form I at 150 °C.

Beyond these studies, Park et al. [20] and Tang et al. [21] reported single crystal XRD data. The sample studied by the former was obtained by slow evaporation from an acetonitrile solution at room temperature. The unit cell parameters reported by both these investigators are also reported in Table 1.

On comparing the results reported in all of these studies, it is clear that there is a lack of consensus on the actual crystal structure of the solvent-free polymorphs. Also, the two melting points seen in the DSC curve of a purportedly pure polymorph, Form F-II [6], poses a further conundrum. Therefore, the aim of this work was to bring greater clarity to the situation by a detailed investigation of the polymorphic behaviour of fipronil using TGA, DSC, PXRD, single crystal XRD (SCXRD) and hot stage microscopy (HSM) as complementary investigative tools.

## Materials and methods

### Materials

Table 2 lists the chemicals used in the study, some of their physical properties and the suppliers. All compounds were used as received, i.e. without further purification. However, a pure form of fipronil was prepared by a sublimation procedure.

### Methods

#### Sample preparation and characterization

A portion of the as-received neat fipronil was purified using vacuum sublimation at approximately 180 °C. The vapour was condensed as purified compound on a cold finger and collected for analysis (Fig. 1b).

Approximately 50 mg of the as-received neat fipronil was dissolved in 4 mL of solvent (acetone, acetonitrile, ethyl acetate or methanol) in a glass vial. The solution was stirred until the fipronil was completely dissolved, after which the solution was left open to air at room temperature (*ca.* 23 °C)

**Table 1** Single crystal data and DSC information for fipronil polymorphs reported in literature

| Crystalline modification | Crystal system space group* | Unit cell parameters | DSC event#/°C | Reference |
|---|---|---|---|---|
| CM-I | Monoclinic<br>*C*2/*c* | *a*—22.2462 Å<br>*b*—12.7041 Å<br>*c*—14.6262 Å<br>α—90°<br>*β* —128.8891°<br>*γ*—90°<br>*Z* = 8<br>*ρ*—1.81 g·cm$^{-3}$ | m.p. 196 – 198↓<br>$T_p$ = 196 | [17] |
| CM-II | Monoclinic<br>$P2_1/c$ | *a*—8.6061 Å<br>*b*—26.9192 Å<br>*c*—16.0861 Å<br>α—90°<br>*β*—102.0661°<br>*γ*—90°<br>*Z* = 4<br>*ρ*—0.94 g·cm$^{-3}$ | 130↓<br>196↓, 203↓ | [18] |
| CM-IV | Triclinic<br>*P*-1 | *a*—8.6461 Å<br>*b*—13.0931 Å<br>*c*—16.6862 Å<br>*α*—99.2021°<br>*β*—103.2251°<br>*γ*—99.5691°<br>*Z* = 2<br>*ρ*—1.64 g·cm$^{-3}$ | 128↓<br>196↓, 203↓ | [16] |
| CM-V | Triclinic<br>*P*-1 | *a*—8.6764 Å<br>*b*—9.1644 Å<br>*c*—11.3674 Å<br>*α*—90°<br>*β*—87.2168°<br>*γ*—83.4508°<br>*Z* = 2<br>*ρ*—1.73 g·cm$^{-3}$ | m.p. 201 – 204<br>203↓ | [7] |
| | Monoclinic<br>*C*2/*c* | *a*—22.564916 Å<br>*b*—12.68239 Å<br>*c* —14.905111 Å<br>*β*— 129.6993°<br>*Z* = 8 | | [20] |
| | Monoclinic<br>$P2_1/n$ | *a* —10.78018 Å<br>*b*—12.70069 Å<br>*c* – 12.10399 Å<br>*β*—96.9731°<br>Z = 4<br>*ρ*—1.701 g·cm$^{-3}$ | | [21] |

*a*, *b*, *c* are the lengths of the unit cell edges; *α*, *β*, *γ* are the angles of the unit cell, *Z* represents the number of molecules in the unit cell and ρ is the calculated density

#↓ denotes an endotherm and ↑ an exotherm

$T_p$: The peak temperature

to allow for evaporation of the solvent until crystallization. The process took 12 to 36 h. Regular inspection of the setup allowed for the identification of the best time to harvest crystals.

Good quality single crystals were collected and analysed using single crystal X-ray diffraction (SCXRD). Crystallization from acetonitrile yielded mixtures of three different crystal forms. This was not the case for the other solvents. Each of the remaining samples were separately homogenised into a powder and analysed by powder X-ray diffraction (PXRD), thermogravimetric analysis (TGA) and differential scanning calorimetry (DSC). The samples were heat treated in a laboratory convection oven for 30 min at either 110 °C or 150 °C to drive off any co-crystallized solvent before analysing by PXRD, TGA and DSC.

**Table 2** Solvents used for recrystallization

| Solvent | CAS No | Molar mass/g $mol^{-1}$ | Density/g $cm^{-3}$ | $T_b$/°C | Purity/% | Supplier |
|---|---|---|---|---|---|---|
| Acetone | 67–64–1 | 58.08 | 0.791 (25 °C) | 56 | ≥99.5 | Sigma-Aldrich |
| Acetonitrile | 75–05–8 | 41.05 | 0.78 (25 °C) | 81.6 | ≥99.5 | Ace Chemicals |
| Ethyl acetate | 141–78–6 | 88.11 | 0.90 (20 °C) | 76.5–77.5 | ≥99.5 | Sigma-Aldrich |
| Methanol | 67–56–1 | 32.04 | 0.79 (20 °C) | 64.7 | ≥99.5 | Sigma-Aldrich |
| Fipronil | 120,068–37-3 | 437.15 | 1.48—1.63 | – | 96 | Avima |

$T_b$: boiling temperature

### Single crystal X-ray diffraction (SCXRD) analysis

X-ray diffraction data of all single crystals were collected at 150.0(2) K using monochromatic Cu-Kα radiation ($\lambda = 1.54184$ Å) on a Rigaku XtaLAB Synergy R diffractometer with a rotating-anode X-ray source and a HyPix CCD detector. Data integration, reduction and multi-scan absorption corrections were performed using the CrysAlisPro (Version 1.171.40.23a) software package [22]. The crystal structures were solved by direct methods or by intrinsic phasing using SHELXT-2013 [23], as part of the WinGX suite [24]. Structure refinements were done using SHELXL [25] in WinGX [24] as GUI. Graphics and publication material were generated using Mercury 3.5 [26]. All H atoms (apart from those of the water molecule in the structure of PM3) were placed in geometrically idealized positions and constrained to ride on their parent atoms. The hydrogen atoms of the water molecule in PM3 could not be placed manually by means of residual electron density, and hence was fixed in positions to allow for the maximum number of hydrogen bonding interactions. In the structure of PM1, no molecule of acetonitrile or related solvent could reliably be modelled within the solvent accessible voids, and therefore was treated as a diffuse contribution to the overall scattering without specific atom positions using the SQUEEZE/PLATON program [27]. The X-ray crystallographic coordinates for all structures have been deposited at the Cambridge Crystallographic Data Centre (CCDC), with deposition numbers CCDC 2,216,777–2,216,781. The data can be obtained free of charge from The Cambridge Crystallographic Data Centre via www.ccdc.cam.ac.uk/data_request/cif.

### Powder X-ray diffraction (PXRD) analysis

PXRD was run on bulk fipronil samples and products of this study mainly to identify and compare data with polymorphs previously reported in literature, as well as supplement interpretation of the DSC results. Some of the PXRD patterns were collected from 5° to 90° on a PANalytical X'Pert Pro powder diffractometer with X'Celerator detector and variable divergence and fixed receiving slits with Fe-filtered Co-Kα radiation. However, the results are reported reflecting 2θ values expected for Cu-Kα radiation. In certain instances, PXRD patterns were also measured at room temperature, on a Bruker D2 Phaser powder diffractometer, employing a Si low-background sample holder, and Cu-Kα radiation.

### Thermogravimetric analysis (TGA)

Thermogravimetric analysis was performed on a TA Instruments Q600 SDT. A multipoint temperature calibration was performed using indium, zinc and gold calibration standards. Mass calibration was carried out using the mass calibration set supplied by the manufacturer. Approximately 10 mg of sample was placed in a 40 µL alumina pan and was heated from ambient temperature to 300 °C at a heating rate ($\beta$) of 2 °C $min^{-1}$ under a nitrogen atmosphere, controlled at a flow rate of 50 mL $min^{-1}$. Analyses were performed in duplicate to confirm the observed effects.

### Differential scanning calorimetry (DSC) analysis

Differential scanning calorimetry analysis was performed on a Mettler Toledo DSC 1. Temperature calibration was performed using indium and zinc calibration standards. Approximately 8 mg of sample was enclosed in 40 µL aluminium pans with pin-holed lids. The temperature was scanned from 25 °C to 300 °C at a heating rate of 5 °C $min^{-1}$. Nitrogen flow was controlled at a rate of 50 mL $min^{-1}$. The effect of varying the heating rate on the DSC curves for the as-received neat fipronil sample was studied in a similar fashion.

Heat-cool-heat analysis was carried out by heating the samples at 5 °C $min^{-1}$ up to 200 °C, a temperature that is just higher than the first endothermic peak but lower than the second endotherm. The samples were immediately cooled down to 100 °C at a rate of 5 °C $min^{-1}$ and then reheated to 300 °C. The same procedure was repeated but with the first heating terminated at 208 °C, a temperature just after the second endotherm.

### Hot stage microscopy (HSM)

HSM was performed on a Linkam Scientific CSS450 heating stage fitted with a Leica DM2500M optical microscope connected to a Leica DFC420 digital camera. About 1 to 2 mg of sample was heated at 5 °C $min^{-1}$ up to 150 °C and then at 2 °C $min^{-1}$ from 150 to 200 °C.

## Results and discussion

### Thermogravimetric analysis (TGA)

Figure 2 shows the TGA and DTG curves for samples obtained by recrystallization from acetone, acetonitrile and methanol.

The TGA and DTG curves for the acetonitrile-derived sample showed an initial mass loss between 60 °C and 100 °C. A similar minor mass loss, ascribed to removal of the solvent, occurred in the acetone-derived sample and in the sample recrystallized from ethyl acetate (not shown). However, for the acetone-derived sample, loss of solvent only occurred between 115 °C and 145 °C. Saxell et al. [16] also commented on the observation that acetone is only removed at temperatures above 120 °C during TGA analysis. This was surprising since the boiling point of acetone (56 °C) is lower than the boiling points of the other recrystallizing solvents (Table 2). Nevertheless, the other solvents were all lost at much lower temperatures. The absence of a mass loss event below 150 °C for the methanol-derived sample indicated that a solvate did not form by recrystallization from methanol. The TGA curves obtained for the as-received neat fipronil, the fipronil sublimate and the heat-treated fipronil samples were similar to that of the methanol-derived material.

Zamir [6] suggested that fipronil forms hemi-solvates with some solvents, i.e. that the solvates contain one molecule of the solvent for every two molecules of fipronil. The ratio of the number of fipronil molecules to solvent molecules of the samples recrystallized in this study was estimated from the TGA mass loss values recorded at a temperature of 150 °C. The ratios estimated for triplicate TGA measurements of the acetone derived sample were 2.23, 2.91 and 3.07; for acetonitrile they were 2.00, 3.25 and 3.39 while for ethyl acetate a value of 2.11 was found. The lower measured values were close to two, the value expected for a hemi-solvate. However, some values were somewhat higher, suggesting that if hemi-solvate formation were indeed possible, the available spaces inside the fipronil channels of some of the present samples were not fully occupied by guest solvent molecules.

Slow mass loss, due to sublimation [28], commenced at temperatures just above 150 °C for all samples. This was also the case for the purified fipronil obtained by sublimation. Figure 1b shows that this produced a white, fluffy powder on the cold finger of the sublimation apparatus. Rapid mass loss, attributed to evaporation, was seen in the TGA curves of all samples once the temperature exceeded 190 °C. However, a thermally stable char residue remained after about 250 °C implying thermal decomposition. The char yield varied from about 6% by mass for the acetonitrile- and acetone-derived samples to as much as 20% by mass for the methanol-derived fipronil sample (Fig. 2a).

### DSC analysis of fipronil

#### DSC analysis of neat fipronil, the sublimate and sublimation residue

Figure 3 shows the DSC curves recorded for the as-received neat fipronil, the purified sublimate and the residue which remained at the bottom of the flask after incomplete sublimation.

The DSC curve of the as-received neat fipronil showed four thermal transitions during heating. The first

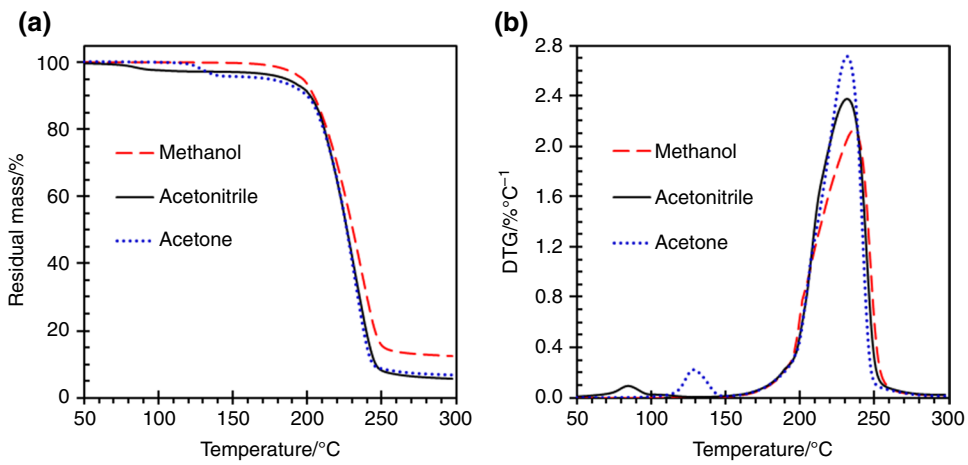


**Fig. 2** **a** Thermogravimetric (TGA) and **b** differential mass change (DTG) curves for fipronil samples recrystallized from acetone, acetonitrile and methanol. $\beta = 2$ °C $min.^{-1}$

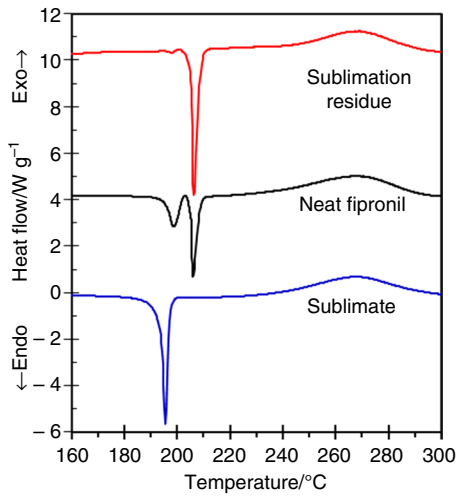


**Fig. 3** DSC curves obtained for neat fipronil, the sublimate and recovered residue from the sublimation experiment. $\beta = 5$ °C min.$^{-1}$

endothermic peak, attributed to melting, occurred with an onset at 193.2 °C, peak maximum at 197.0 °C and $\Delta H_m = 21.2$ J g$^{-1}$. This was followed by a small exothermic event at ~ 202 °C ($\Delta H_c = -5.1$ J g$^{-1}$), attributed to recrystallization of the melt. Immediately thereafter, a second endothermic transition with a peak temperature of 206.0 °C and $\Delta H_m$ of 87.1 J g$^{-1}$, due to a second melting process, was observed. The fourth transition was a broad exotherm with an onset at 246 °C and peak maximum at 260 °C due to the decomposition of fipronil. The presence of two melting endotherms, which were also observed on a hot stage microscope, may indicate the presence of a mixture of two polymorphic forms in the neat fipronil sample. This data confirmed that of Zamir (2013), who suggested that pure Form F-II (similar to CM-I reported by Saxell [7]) exhibited two melting endotherms. However, Saxell et al. [16, 17] was able to prepare a sample of crystalline modifications CM-I which featured a single melting endotherm with a peak maximum between 196—199 °C [17]. In the current study, the sublimate and sublimation residue were identified by PXRD as the polymorphs CM-I and CM-V, reported by Saxell [7], respectively. The sublimate sample formed at low temperatures as it was collected on the cold finger. It featured a lower melting point (195.4 °C) than the sublimation residue (206.1 °C) which was, in effect, heat-treated at about 180 °C during the sublimation experiment.

Table 3 summarises the DSC parameters (temperature and enthalpy values) of the observed transitions for the neat fipronil, the purified sublimate and the residue which remained at the bottom of the flask after incomplete sublimation.

Figure 4 shows the effect of varying the heating rate on the DSC curves of neat fipronil. The heating rate is a decisive parameter which can determine the extent and mechanism of polymorphic transformation [25].

At low heating rates (1–2 °C min$^{-1}$), a small endotherm was observed at ~ 188 °C followed by a sharp melting peak centred at ~ 203 °C. As the heating rate was increased, the small endotherm shifted to higher temperatures and increased in intensity. Simultaneously, the relative intensity of the second endotherm decreased. At intermediate heating rates (4–8 °C min$^{-1}$), two well-defined melting endotherms separated by a small exotherm were noticeable. At high heating rates (60–80 °C min$^{-1}$) the two melting endotherms merged until eventually only one broadened peak was left. This unexpected behaviour can be rationalised as follows.

**Table 3** DSC parameters obtained for different fipronil samples

| Sample | $T_s$ onset/°C | $T_s$ peak/°C | m.p. onset/°C | $T_{m1}$/°C | $T_{m2}$/°C | $\Delta H_{m1}$/J·g$^{-1}$ | $\Delta H_{m2}$/J·g$^{-1}$ |
|---|---|---|---|---|---|---|---|
| Neat | – | – | 193.2 | 197.0 | 205.8 | 21.2 | 87.1 |
| Neat (150)* | – | – | 193.8 | 196.3 | 204.6 | 17.3 | 89.9 |
| Sublimate | – | – | 193.3 | 195.4 | – | 96.8 | – |
| Sublimate residue | – | – | | – | 206.1 | – | 95.3 |
| Acetone | 129.9 | 136.8 | 193.8 | 197.0 | 205.3 | 14.7 | 92.5 |
| Acetone (110) | – | – | 194.1 | 196.8 | 205.0 | 18.6 | 81.0 |
| Acetonitrile | 93.7 | 97.1 | 195.4 | 198.5 | 205.3 | 65.6 | 32.9 |
| Acetonitrile (110) | – | – | 193.6 | 197.4 | 203.6 | 90.7 | 19.5 |
| Acetonitrile (150) | – | – | 194.1 | 196.9 | 205.4 | 1.4 | 101.0 |
| Ethyl acetate | – | – | 196.4 | 198.1 | – | 78.2 | – |
| Ethyl acetate (150) | – | – | 194.7 | – | 206.0 | – | 101.5 |
| Methanol | – | – | 195.6 | 198.6 | – | 100.5 | – |
| Methanol (110) | – | – | 196.8 | 198.5 | – | 100.8 | – |

$T_s$: desolvation temperature; $T_{m1}$ and $\Delta H_{m1}$: temperature and enthalpy change associated with the first melting endotherm

$T_{m2}$ and $\Delta H_{m2}$: temperature and enthalpy change associated with the second melting endotherm

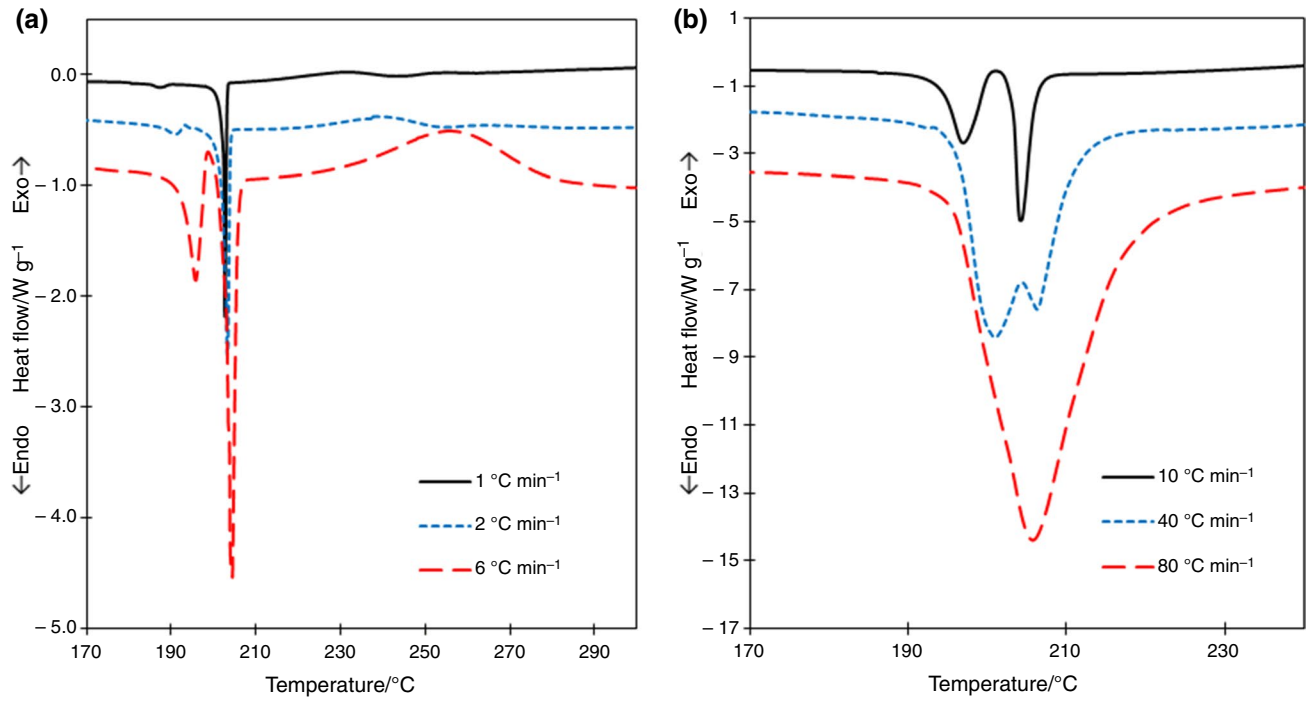


**Fig. 4** The effect of heating rate on the DSC curves for neat fipronil

Polymorph CM-I (the lower melting form) is the metastable form which undergoes either a solid–solid transition or melting and recrystallization to the thermodynamically stable form, polymorph CM-V (the higher melting form). The metastable form has a finite existence due its slow rate of transformation into the stable form [29]. One explanation for the small endotherm that was detected around 190 °C at lower heating rates (1–2 °C $min^{-1}$), is the occurrence of a solid phase transition CM-I → CM-V at a temperature well below the melting point of polymorph CM-I. When heated slowly, a low melting metastable polymorph usually transitions to the higher melting polymorph at an appropriate temperature. However, under rapid heating conditions it tends to overshoot and melt at its own melting point [1, 30]. Therefore, complete conversion of CM-I into the stable CM-V polymorph was only achieved at a low heating rate. At intermediate heating rates, the solid transformation CM-I → CM-V did not occur. Instead, CM-I melted. Once the metastable polymorph melted, the resulting melt crystallized to form the higher melting, stable polymorph CM-V. This explains the exotherm present at intermediate heating rates. This phenomenon can serve as another explanation for the small endotherm observed at around 190 °C at lower heating rates (1–2 °C $min^{-1}$). The gradual dissipation of the heat of fusion over time could have led to a recrystallization exotherm with a very low intensity that was undetectable on the DSC.

As the heating rate was increased further, less of the higher melting polymorph (CM-V) had time to form. This explains the variation in the relative intensities of the two melting endotherms with DSC heating rate (Fig. 4). It also explains why polymorph F-II reported by Zamir [6] (cf. polymorph CM-I) appeared to have two melting points. It is simply an artefact caused by a solid–solid phase transformation of CM- I into CM-V, the stable polymorph. At a high heating rate of 80 °C $min^{-1}$, formation of the stable form was suppressed and only the melting endotherm of the metastable form was observed.

### DSC analysis of the solvates

Representative DSC curves for the fipronil solvates, before and after heat-treatment, are shown in Fig. 5. The measured onset and peak temperatures are listed in Table 3. Weak endothermic events were present in the DSC curves of some samples at temperatures below 150 °C. These endotherms reflected the release of the solvents, acetone, acetonitrile and ethyl acetate, present in the initial structures. The methanol-derived sample did not feature such an event.

At relatively high temperatures, all the samples exhibited a broad exotherm which peaked between 260 °C and 280 °C. This was attributed to the degradation of fipronil, also observed in the TGA experiments. The TGA results indicated that degradation of fipronil led to the loss of volatile

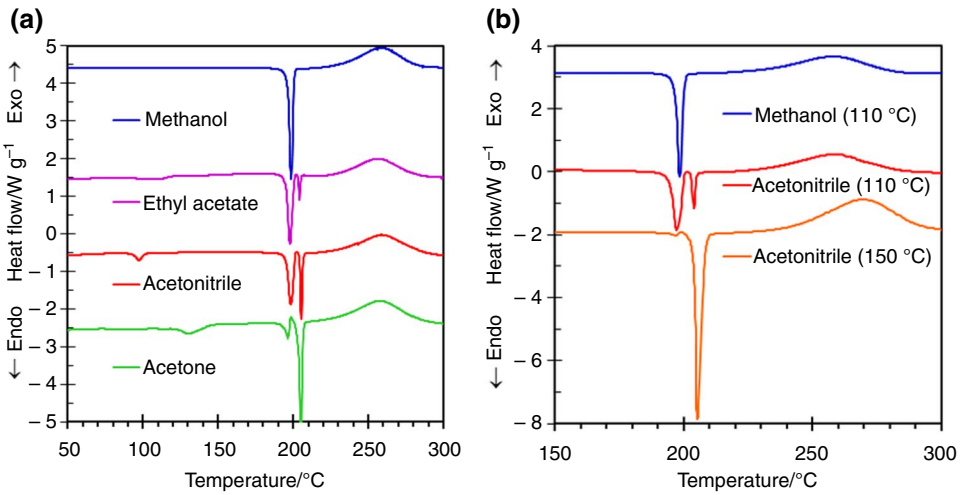


**Fig. 5** DSC curves obtained for **a** fipronil samples prepared by recrystallization from different solvents, and **b** after heating to either 110 °C and 150 °C. $\beta = 5$ °C min$^{-1}$

decomposition products and the formation of a thermally stable char residue (Fig. 2).

Figure 5a shows that the methanol-derived sample is characterized by a single sharp melting endotherm with onset at 195.6 °C and peak temperature of 198.6 °C. Figure 5b shows that heat treatment of the methanol derived-sample at 110 °C for 10 min did not change the melting behaviour of this sample. In contrast, all the other examples, shown in Fig. 5a, featured two melting endotherms with the second endotherm located at a temperature slightly higher than 200 °C. Both melting events featured quite sharp peaks but they varied in relative intensity for the different samples. For the acetone- and acetonitrile-derived samples, the second melting event was the most intense whereas the reverse held for ethyl acetate-derived sample.

The effect of heat treatment of the acetonitrile-derived sample was particularly striking when comparing the DSC results of the sample before and after heat treatment. First compare the DSC curve for the solvate (Fig. 5a) and the sample heat treated at 110 °C (Fig. 5b). The first endotherm became more intense following the heat treatment ($\Delta H_{m1}$ values 65.6 J g$^{-1}$ *vs* 90.7 J g$^{-1}$; Table 3). However, when the acetonitrile-derived sample was heated for 30 min at 150 °C, the second melting event became dominant and only a vestige of the first remained. This was consistent with near complete transformation into the thermodynamically stable CM-V polymorph and implied that the solid–solid phase transformation temperature of the metastable polymorph must be below 150 °C.

The implication of the results presented above is that the ultimate phase morphology of fipronil depends on the solvents used in its preparation as well as on the thermal history it was subjected to. In order to investigate the latter, a series of heat-cool-reheat DSC runs were conducted. Figure 6 shows typical behaviour observed for the different samples. In the first set of experiments, the samples were heated up to 200 °C, a temperature just beyond the first melting endotherm but before the onset of the second one, followed by immediate cooling down to 100 °C and then reheating to 300 °C. Heating any of the fipronil samples in this way resulted in them having only a single melting endotherm in the range 205 °C to 207 °C (Fig. 6a, c). This suggested that such a thermal treatment leads to an irreversible phase transition of crystalline modification CM-I to crystalline modification CM-V, and confirmed that polymorph CM-V is the stable polymorph at elevated temperatures.

A similar procedure was carried out with the initial heating scan reaching 208 °C, a temperature just after the second endotherm (Fig. 6b, d). After rapidly cooling and then reheating, the DSC curve showed two endotherms, a major endotherm centred at 181.2 °C and a minor one centred at 197.3 °C. The minor endotherm at 197.3 °C corresponds to the melting range of polymorph CM-I while the endotherm at 181.2 °C is most likely due to a lower-melting degradation product of fipronil.

## Powder X-ray diffraction

Powder X-ray diffraction results were employed in an attempt to confirm the associations, made on the basis of DSC results, between the various preparations and specific polymorphs mentioned in the literature. Figure 7 compares the PXRD patterns obtained from methanol- and acetonitrile-derived fipronil following heat treatment of both samples at 150 °C. The diffractogram obtained for the methanol-derived fipronil, heat treated at 150 °C, compares very well with the patterns published by Saxell's for CM-I [17] and Zamir's for F-II [6]. The diffractograms recorded for all the other samples of fipronil (neat, sublimated and heated at 150 °C) as well as all samples, before and after heat-treatment at 110 °C, obtained by recrystallization from acetone, ethyl acetate, toluene or methanol were also very similar

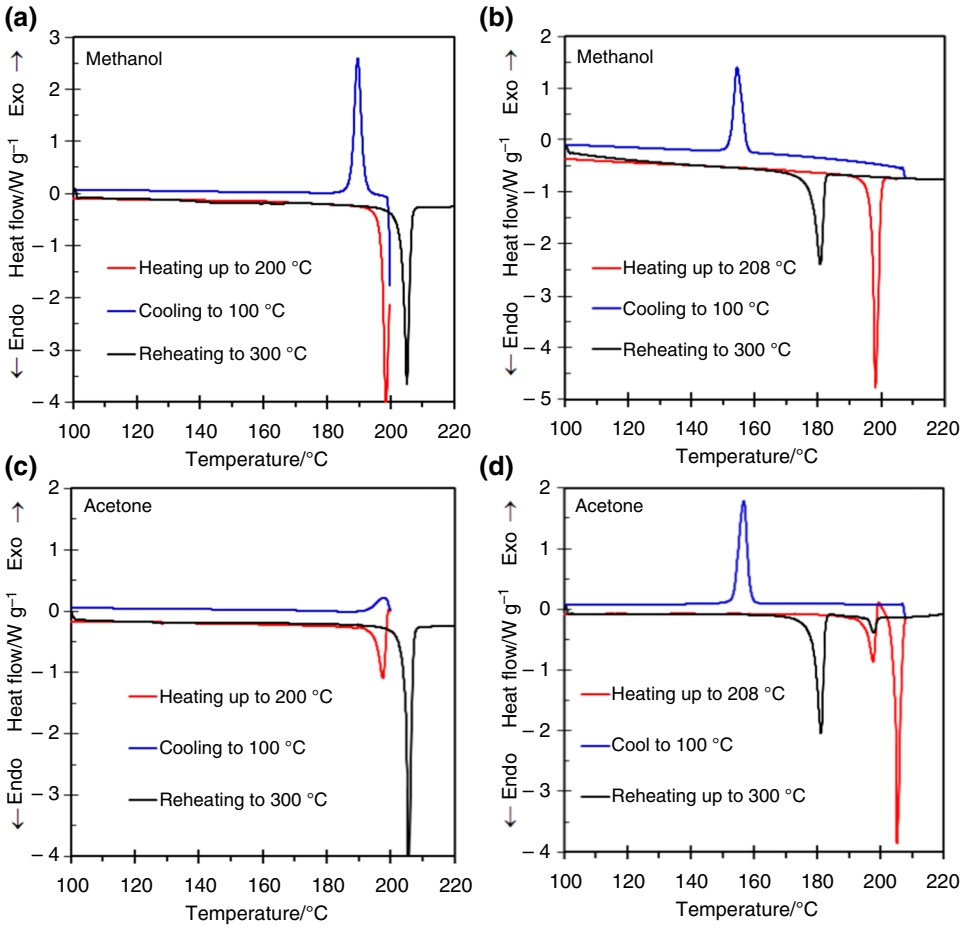


**Fig. 6** The effect of two different heat-cool-heat protocols on the DSC curves of fipronil samples obtained by recrystallization from methanol **a** and **b**, and acetone **c** and **d**. $\beta = 5$ °C min.$^{-1}$.

as they appeared to be dominated by the reflections typical for CM-I or FII. This implied that most contained very high proportions of this polymorph. The PXRD pattern for the sample obtained by heat treatment of the acetonitrile-derived sample at 150 °C for 30 min corresponded to that of CM-V and F-I reported by Saxell et al. [7] and Zamir [6], respectively.

## Crystal structure analysis

The powder XRD patterns do not reflect the characteristics of the individual pure phases as some of the samples were, to some extent, mixtures of the various polymorphs. However, it was possible to pick out single crystals from some of the recrystallized fipronil samples and subject them to SCXRD analysis. Five different crystalline forms (polymorphs or pseudo-polymorphs) of fipronil were identified using SCXRD data. These were labelled PM-1 to PM-5. The crystals of forms PM-1 and PM-2 were obtained from acetonitrile, PM-3 was obtained from acetone, PM-4 was crystallized from ethyl acetate, while crystals of PM-5 were grown from methanol. PM-5 was found to correspond to the polymorph reported previously in the literature by Park et al. [20]. Table 4 lists the crystallographic parameters of the different structures. Figure 8 illustrates the asymmetric units of PM-1 to PM-5, with packing diagrams shown in Fig. 9. The hydrogen bonding networks present in PM1-PM5 are illustrated in Fig. 10.

### Form PM-1

PM-1 was obtained by crystallization from acetonitrile at room temperature. This form was similar to Saxell's crystalline modification CM-II. The pseudo-polymorph crystallizes in the space group $P2_1/c$, with the asymmetric unit comprised of two crystallographically independent fipronil molecules, as shown in Fig. 8a, with the molecule containing atom S1 labelled molecule A, and the molecule containing atom S2 denoted molecule B. In both molecules A and B, the trifluoromethyl group attached to the benzene ring is disordered over two positions, with relative occupancies of 0.781(11) and 0.219(11) in molecule A and 0.56(2) and 0.44(2) in molecule B. In molecule A, the planes through the benzene and pyrazole groups form an angle of 81.25°, with the corresponding angle having a value of 78.55° in molecule B. These relative

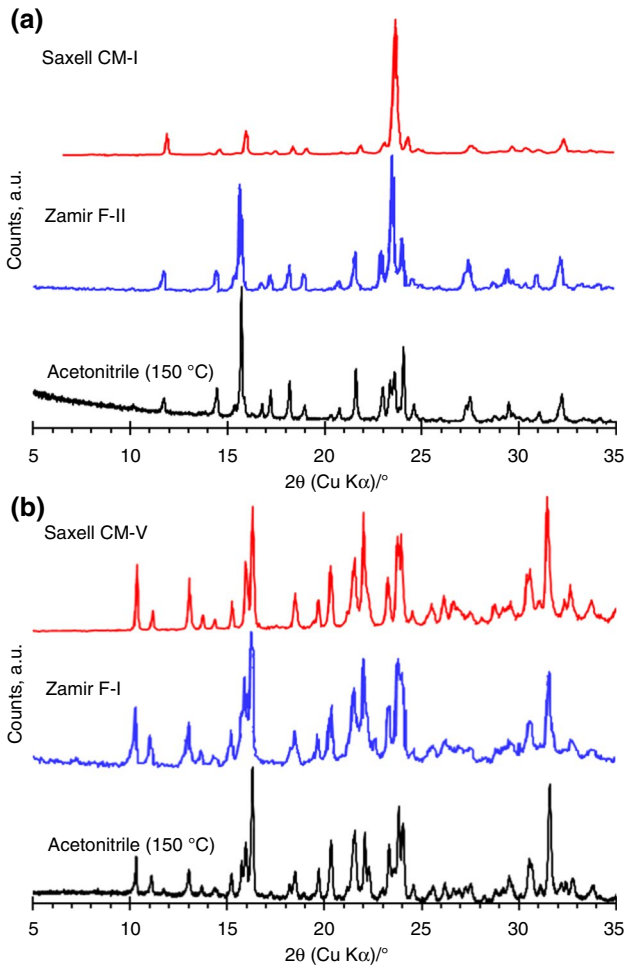


**Fig. 7** Powder X-ray diffractograms for heat treated fipronil samples obtained by recrystallization from **a** methanol and **b** acetonitrile. For comparison, the patterns of solvent-free fipronil polymorphs reported by Saxell [7, 17] and Zamir [6, 19] are also shown.

ring orientations, leaning towards 90°, are primarily due to steric effects where the 2,6-dichloro substituents on the aryl ring would come into close contact or even overlap in space with the $NH_2$ substituent and N3-atom of the pyrazole ring in the case of the two planes bisecting at 0°. In general, the bonding distances of the respective functional groups all fall within the expected ranges [20].

Figure 9a illustrates the packing of the molecules as viewed down the *a*-axis. It is evident, from the packing diagram, that channels are present in the structure. These are assumed to be occupied by acetonitrile solvent molecules, making PM-1 a pseudo-polymorph of fipronil. However, the acetonitrile solvent molecules could not be located reliably in the electron difference map, hence the SQUEEZE command was employed in the refinement of the structure where the diffuse contribution to the overall scattering of one molecule of acetonitrile was considered.

In both molecules A and B, each $NH_2$ group (N1) forms two hydrogen bonds. Firstly, a bifurcated hydrogen bond is formed to two oxygen atoms (O1, O2) of two different sulfinyl groups, with one hydrogen bond intramolecular (N1-H1B···O1), and one intermolecular (N1-H1B···O2). The second hydrogen atom on the amine group (N1-H1A) forms an intermolecular hydrogen bond to the nitrogen atom (N4) of a nitrile group on a different molecule. Figure 10a illustrates the resulting hydrogen bonded ribbon. Molecule's A form propagates on the one side of the hydrogen bonded ribbon, and molecule's B form the opposite side of the ribbon. Distinct hydrogen bonding networks may also be described in terms of graph sets: two unique parallel chains (the one involving molecule A and the other molecule B) may each be defined as $C(7)$, whereas the intramolecular hydrogen bond between the amine and sulfinyl group may be defined as $S(6)$. Two unique rings are also observed, the one involving two molecules, $R_2^2(4)$, and a larger ring incorporating four different molecules, $R_4^4(18)$. It is interesting to note that all five structures PM-1 to PM-5 exhibited identical hydrogen bonding patterns and graph sets (vide infra), despite their unique structures and packing in three dimensions. Additionally, one of the hydrogen atoms on the amine group of molecule B forms a hydrogen bond to a chlorine atom on a neighbouring molecule, effectively making this a trifurcated hydrogen bond. This interaction is not observed for molecule A. Hydrogen bonding parameters are listed in Table 5.

### Form PM-2

PM-2 was crystallized from acetonitrile at room temperature and was found to be a concomitant polymorph to PM-1, since it formed in the same crystallization vessel as pseudo-polymorph PM-1. PM-2 crystallizes in the space group $P2_1/c$, and does not contain any solvent molecules, hence it is a polymorph of fipronil.

The asymmetric unit of PM-2 comprises two fipronil molecules, which will be denoted molecule A, containing nitrogen atom S1, and molecule B, containing nitrogen atom S2. Both molecule A and molecule B contain disordered trifluoromethyl groups, however, the two molecules differ in the type of disorder exhibited by the groups. In molecule A the fluorine atoms of the trifluoromethyl group bonded to the benzene group are disordered over two positions, with an occupancy of 0.566(10) and 0.434(1). The entire trifluoromethyl group bonded to the sulphur atom is disordered over two positions in molecule B, with the two disordered portions on opposite sides of the sulphur atom, with occupancies of 0.6 and 0.4, respectively.

The angle between the plane through the benzene group and the plane through the pyrazole group is 81.26° in molecule A and 81.59° in molecule B, which are comparable with those in PM-1.

**Table 4** Crystallographic data of fipronil polymorphs, solvates and hydrates

| Polymorph | PM-1 | PM-2 | PM-3 | PM-4 | PM-5 |
|---|---|---|---|---|---|
| Crystal system | Monoclinic | Monoclinic | Triclinic | Monoclinic | Monoclinic |
| Space group | $P2_1/c$ | $P2_1/c$ | $P\text{-}1$ | $P2_1/c$ | $I2/a$ |
| $a$/Å | 8.5926(2) | 14.5034(3) | 8.65640(10) | 14.7036(4) | 17.3452(2) |
| $b$/Å | 27.0164(14) | 31.1201(6) | 13.1917(4) | 15.5016(6) | 12.6351(2) |
| $c$/Å | 16.0685(5) | 8.71330(10) | 16.7395(4) | 8.6691(2) | 14.9462(2) |
| $\alpha$/° | 90 | 90 | 99.535(2) | 90 | 90 |
| $\beta$/° | 101.026(3) | 93.658(2) | 103.068(2) | 93.796(2) | 91.7830(10) |
| $\gamma$/° | 90 | 90 | 99.579(2) | 90 | 90 |
| Volume/ Å$^3$ | 3661.3(2) | 3924.71(12) | 1794.47(8) | 1971.61(10) | 3274.00(8) |
| Z | 4 | 4 | 2 | 4 | 8 |
| Calculated density/g cm$^{-3}$ | 1.641 | 1.480 | 1.633 | 1.489 | 1.774 |
| Goodness-of-fit on $F^2$ | 1.087 | 1.098 | 1.117 | 1.040 | 1.041 |
| Final $R_1$ index [all data] | 0.1245 | 0.0938 | 0.0921 | 0.1015 | 0.0470 |
| $wR_2$ index [all data] | 0.2712 | 0.2796 | 0.2472 | 0.2580 | 0.1211 |
| $\Delta\rho$ max/min (eÅ$^{-3}$) | 1.16/−0.76 | 1.87/−0.50 | 1.27/−0.68 | 0.65/−0.41 | 0.70/−0.58 |
| Similar structure in literature: | CM-II [18] | – | CM-IV [16] | | Park [20], Saxell [17] CM-I & Zamir F-II [6] |

$a$, $b$, $c$ are the lengths of the unit cell edges; $\alpha$, $\beta$, $\gamma$ are the angles of the unit cell, $Z$ represents the number of molecules in the unit cell and $\rho$ is the calculated density

The packing diagram of PM2 is illustrated in Fig. 9b A sinusoidal, layered packing is exhibited, with benzene groups and their attached substituents packing in a layer, the tetrafluoromethanesulfinyl groups packing in a layer, and the pyrazole groups packing in two different layers.

As illustrated in Fig. 10b, one of the hydrogen atoms of an amine group of molecule A (or molecule B) forms a bifurcated hydrogen bond between its own sulfinyl group, and the sulfinyl group of a molecule B (or molecule A), thus the bifurcated hydrogen bond is both intramolecular and intermolecular. At the same time, the second hydrogen atom on the amine group of molecule A (or molecule B) forms a hydrogen bond to the nitrile group of a different molecule A (or molecule B). These interactions result in a hydrogen bonded ribbon consisting of hydrogen bonded molecules A and B, as illustrated in Fig. 10b.

### Form PM-3

PM-3 crystallizes in the space group P $\bar{1}$, and was obtained from acetone. Its structure was found to contain solvent water molecules, which were presumed to have been present in the acetone solvent used for crystallization, making it a pseudo-polymorph of fipronil. PM-3 is a hemihydrate of fipronil. A similar form was obtained by Saxell and co-authors [16] and named crystalline modification CM-IV.

The asymmetric unit of PM-3 contains two fipronil molecules and one water molecule, with the fipronil molecules showing disorder in their trifluoromethyl groups (Fig. 8c). The molecule containing atom S1 will be denoted molecule A, and the one containing atom S2 molecule B. In both molecules the fluorine atoms of the trifluoromethyl group on the benzene ring are disordered over two positions, with an occupancy of 0.773(15) and 0.227(15) in molecule A, and 0.457(19) and 0.543(19) in molecule B. In molecule B, the trifluoromethyl group attached to the sulphur atom is disordered over two positions, on opposite sides of the sulphur atom, with an equal occupancy of 0.5 each. The plane through the benzene group and the plane through the pyrazole group form an angle of 80.65° in molecule A and 84.03° in molecule B.

As can be seen from Fig. 9c, a layered structure is formed, with the benzene groups and their attached substituents packing in a layer, the tetrafluoromethanesulfinyl groups packing in a layer, and the pyrazole groups packing in two different layers. The water molecules pack in rows along the $a$-direction.

Exactly the same hydrogen bonding interactions that were found to be present between the fipronil molecules in PM-2, are present in PM-3. These result in a hydrogen bonded ribbon, as depicted in Fig. 10c. Additionally, the water molecules are involved in hydrogen bonding, with each water molecule forming two hydrogen bonds to two different chlorine atoms on two different neighbouring fipronil molecules.

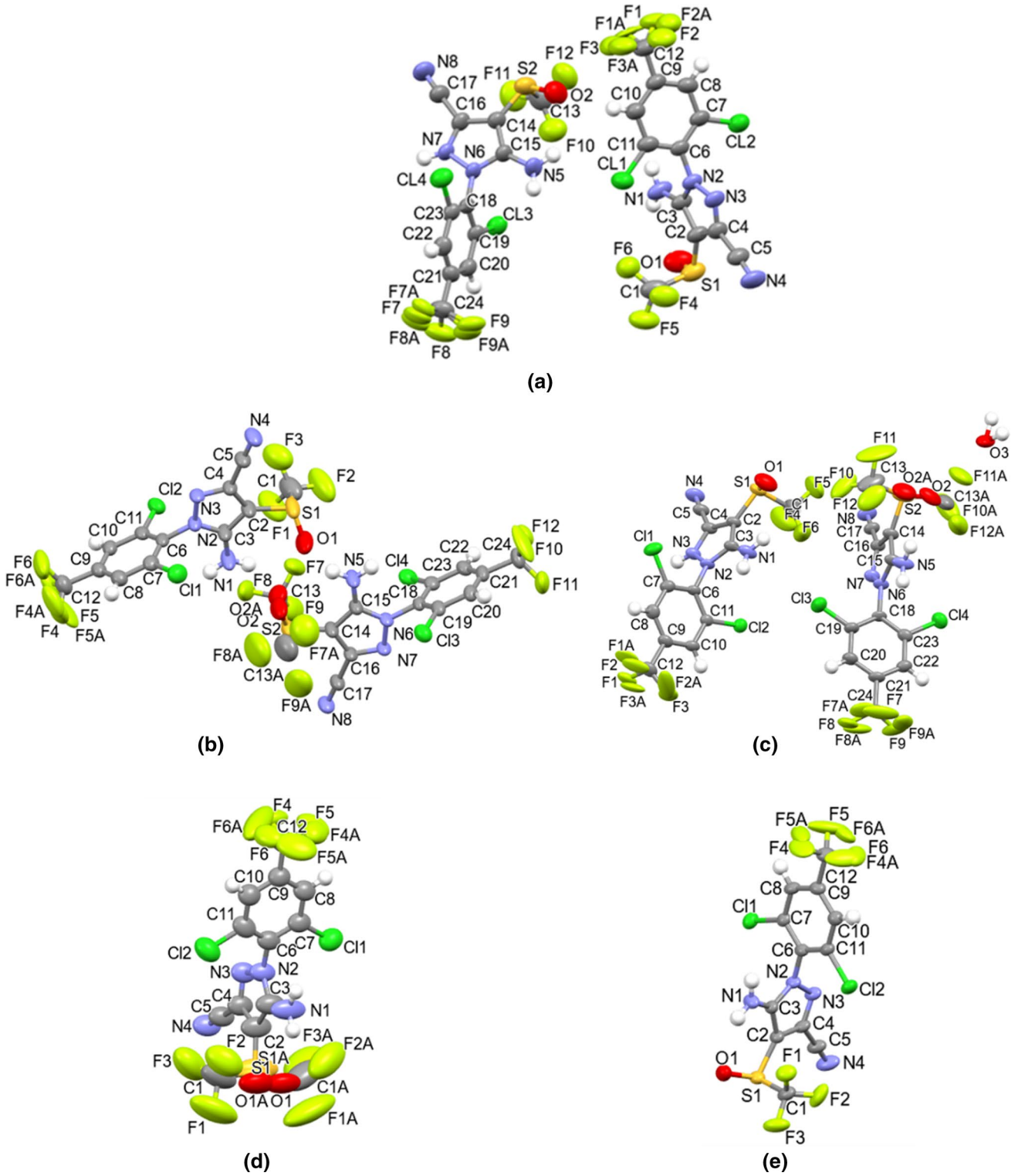


**Fig. 8** Asymmetric units of **a** PM-1 **b** PM-2 (c) PM-3 **d** PM-4 and **e** PM-5. Ellipsoids are drawn at the 50% probability level, and hydrogen atoms are illustrated as white spheres of arbitrary size

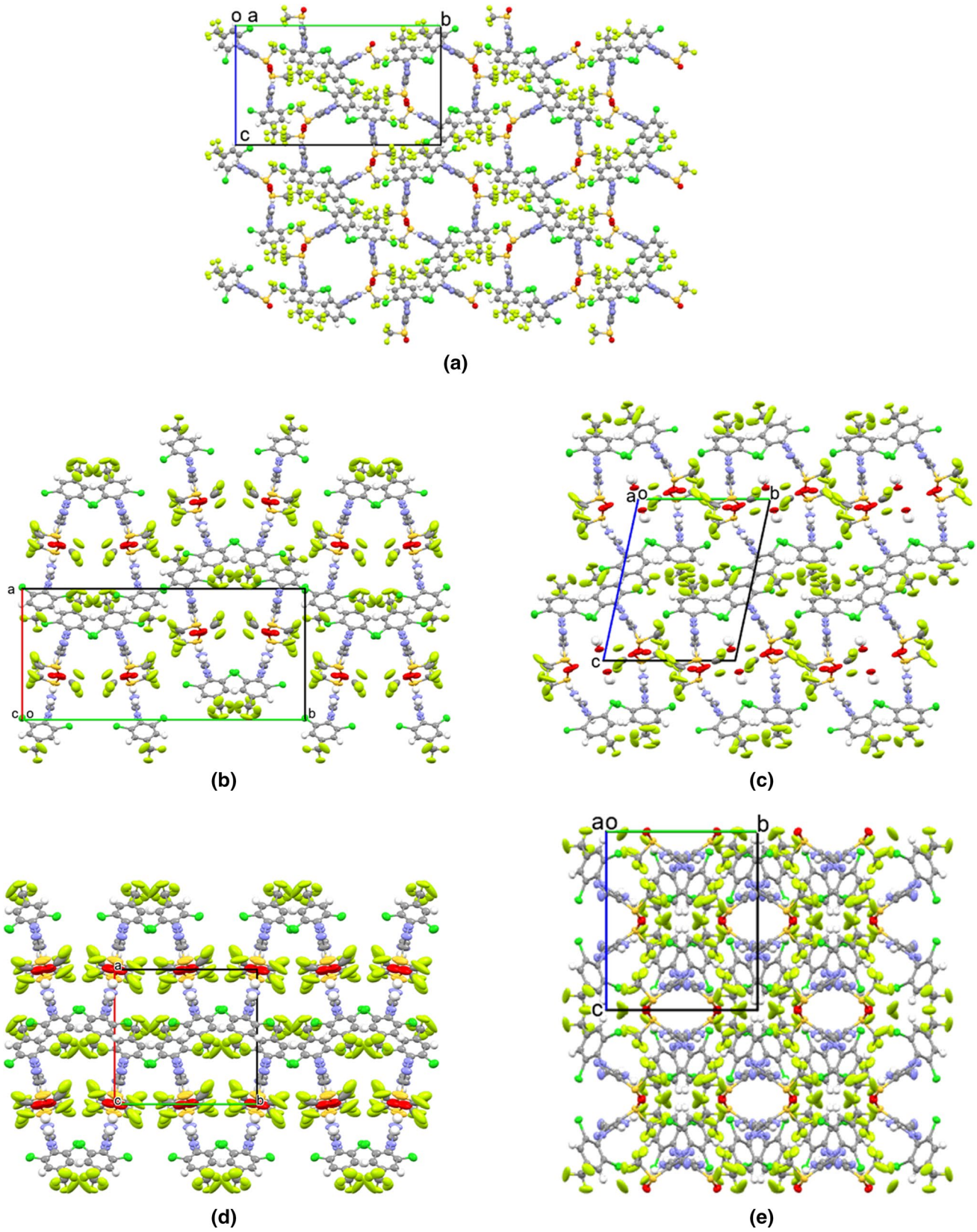


**Fig. 9** Packing diagrams of **a** PM-1 viewed down the *a*-axis **b** PM-2 viewed down the *c*-axis **c** PM-3 viewed down the *a*-axis **d** PM-4 viewed down the *c*-axis and **e** PM-5 viewed down the *a*-axis

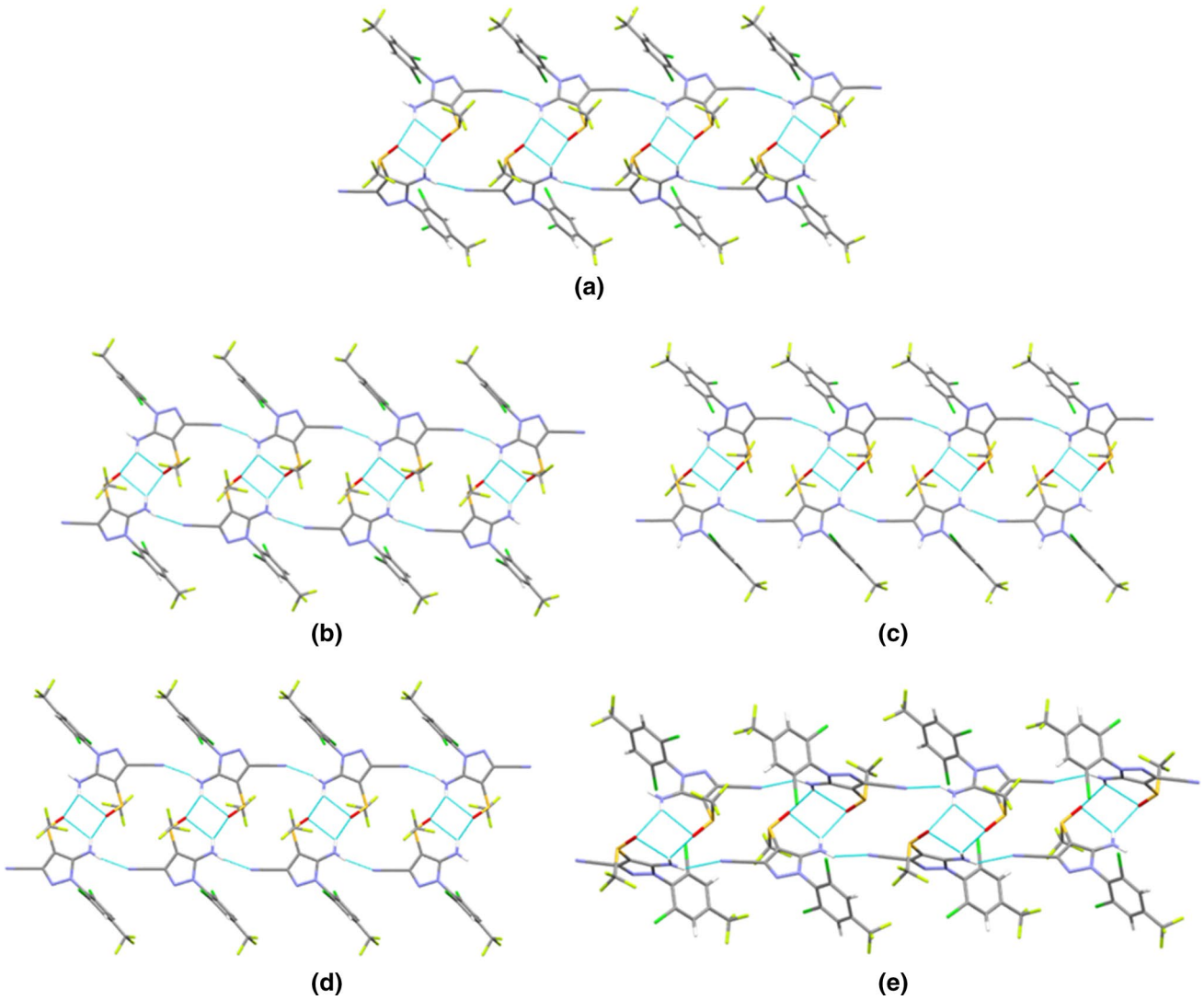


**Fig. 10** Hydrogen bonding interactions in **a** PM-1 **b** PM-2 **c** PM-3 **d** PM-4, and **e** PM-5

### Form PM-4

PM-4 crystallized from acetonitrile at room temperature in the space group $P2_1/c$, with one fipronil molecule in the asymmetric unit. In this molecule, the trifluoromethylsulfinyl group and the fluorine atoms on the trifluoromethyl group on the benzene ring are disordered over two positions, with the first showing an equal occupancy of 0.5, and the second an occupancy of 0.622(8) and 0.378(8). As can be seen in Fig. 8d, the disordered trifluoromethulsulfinyl groups are positioned on opposite sides of the pyrazole plane, with the pyrazole plane forming an angle of 86.78° with the benzene plane.

The packing of fipronil molecules in this polymorph, as viewed down the *c*-axis, is illustrated in Fig. 9d. A layered structure is formed, with the benzyl groups packing in a layer, and the trifluoromethulsulfinyl packing in another layer. The packing of molecules is similar to the packing observed in PM-2, however the layers are more wavy in PM-2.

Identical hydrogen bonding interactions between fipronil molecules in PM-2 and PM-3 are present (Fig. 10d).

### Form PM-5

PM-5 was crystallized from methanol at room temperature and corresponds to the structure of fipronil reported in the literature, with CSD (Version 5.43, September 2022 update) [31] reference code YEGJAY [20]. The literature structure was reported in setting *C*2/*c* of space group 15, however, in the current study it has been determined in the conventional setting *I*2/*a*. Since a detailed discussion of this structure has been published [20], only the major structural features will

**Table 5** Selected hydrogen bonding parameters (Platon) for Polymorphs PM-1 to PM-5

| Form | D-H···A | D-H/Å | H···A/Å | D···A/Å | D-H···A/° | Symmetry |
|---|---|---|---|---|---|---|
| PM-1 | N1-H1A···N4 | 0.8800 | 2.2000 | 3.0647 | 168.00 | −1+x,y,z |
| | N1-H1B···O1 | 0.8800 | 2.4100 | 3.0146 | 126.00 | – |
| | N1-H1B···O2 | 0.8800 | 2.2400 | 2.9996 | 144.00 | x,1/2-y,-1/2+z |
| | N5-H5A···N8 | 0.8800 | 2.1800 | 3.0483 | 168.00 | 1+x,y,z |
| | N5-H5B···O2 | 0.8800 | 2.4100 | 2.9935 | 124.00 | – |
| | N5-H5B···O1 | 0.8800 | 2.2300 | 2.9609 | 140.00 | x,1/2-y,1/2+z |
| PM-2 | N1-H1A···N4 | 0.8800 | 2.2000 | 3.0571 | 166.00 | x,y,1+z |
| | N1-H1B···O2 | 0.8800 | 2.1600 | 2.8862 | 140.00 | - |
| | N5-H5A···N8 | 0.8800 | 2.1700 | 3.0219 | 163.00 | x,y,−1+z |
| | N5-H5B···O2 | 0.8800 | 2.1100 | 2.8811 | 146.00 | – |
| | N5-H5B···O1 | 0.8800 | 2.5500 | 3.1136 | 123.00 | – |
| PM-3 | N1-H1A···N4 | 0.8800 | 2.2100 | 3.0815 | 169.00 | 1+x,y,z |
| | N1-H1B···O2 | 0.8800 | 2.3000 | 2.9184 | 127.00 | x,y,1+z |
| | N1-H1B···O2A | 0.8800 | 2.1800 | 2.9813 | 152.00 | −1+x,y,z |
| | N5-H5A···N8 | 0.8800 | 2.1700 | 3.0309 | 167.00 | x,y,−1+z |
| | N5-H5B···O1 | 0.8800 | 2.0800 | 2.8508 | 146.00 | – |
| | N5-H5B···O2A | 0.8800 | 2.5000 | 3.0861 | 125.00 | – |
| PM-4 | N1-H1A···N4 | 0.8800 | 2.1700 | 3.0305 | 166.00 | x,y,1+z |
| | N1-H1B···O1 | 0.8800 | 2.5400 | 3.1059 | 123.00 | – |
| | N1-H1B···O1 | 0.8800 | 2.1300 | 2.8838 | 144.00 | −x,1−y,1−z |
| | N1-H1B···O1A | 0.8800 | 2.1000 | 2.8784 | 146.00 | −x,1-y,1−z |
| PM-5 | N1-H1A···N4 | 0.8800 | 2.3800 | 3.1728 | 151.00 | −1/2+x,1−y,z |
| | N1-H1B···O1 | 0.8800 | 2.5100 | 3.0909 | 124.00 | – |
| | N1-H1B···O1 | 0.8800 | 2.2800 | 2.8945 | 127.00 | 1/2-x,y,−z |

be highlighted here, especially with reference to the other polymorphs or pseudo-polymorphs.

The asymmetric unit of PM-5 is comprised of one fipronil molecule, with the trifluoromethyl group on the benzene ring disordered over two positions, with occupancies of 0.611(16) and 0.389(16). Interestingly, the same disorder is present in the structure in YEGJAY, where they found occupancies of 0.620(15) and 0.380(15). In the structure of PM-5, the plane through the benzene group and the plane through the pyrazole group form an angle of 89.69°, closely corresponding to the same angle in YEGJAY (89.03(9)°). This angle is the closest to 90° of all the plane dihedral angles in forms PM-1 to PM-5, with molecule A of PM-3 having the smallest angle of 80.65°.

The packing diagram of fipronil molecules in PM-5, viewed down the *a*-axis, is shown in Fig. 9e. Channels extending along the *a*-direction is evident from packing along the *a*-axis. It is presumed that these channels were occupied by methanol solvent molecules during crystallization, evaporating over time leaving the crystal lattice intact. The precise location of the solvent molecules could not be placed in the electron density map due to little or no density observed in the voids. The same hydrogen bonding interactions present between fipronil molecules in PM-1 to PM-4 are present in PM-5, as illustrated in Fig. 10e.

## Conclusions

The aim of this study was to reconsider the crystallography and thermal properties of fipronil polymorphs and pseudo-polymorphs in the hope of finding a resolution to these differences. Therefore, samples of fipronil as-received, purified by sublimation and by recrystallization from solvents, were studied by means of DSC, TGA, PXRD, SCXRD and hot stage microscopy.

In this study five different forms were identified using SCXRD. Concomitant polymorphism was observed when fipronil was crystallized from acetonitrile or ethyl acetate at room temperature. Forms PM-1, PM-2 and PM-5 crystallized from the first solvent, and forms PM-1, PM-4 and PM-5 from the second. Crystallization from acetone at room temperature was found to exclusively yield PM-3, while PM-5 was exclusively obtained from crystallization from methanol at room temperature. Pure PM-4 was obtained by crystallizing from acetonitrile cooled in a refrigerator.

Despite recrystallization from acetonitrile giving a mixture of different polymorphs/pseudo-polymorphs, heat treating this product for 30 min at 150 °C resulted in a near-pure polymorph with PXRD and thermal behaviour consistent with crystal modification CM-V described by Saxell et al. [7] and form F-I reported by Zamir [6]. TGA

results showed that recrystallization from methanol does not yield a solvate. Instead, a near-pure polymorph, named PM-5, was obtained with PXRD properties similar to those for crystal modification CM-I reported by Saxell et al. [17] and Form F-II disclosed by Zamir [6]. Its PXRD pattern also closely resembled the one predicted on the basis of the single crystal data published by Park et al. [20]. All investigators agreed that this polymorph belongs in the monoclinic crystal system. However, the present analysis indexes this polymorph into space group *I*2/*a* whereas Tang et al. suggested $P2_1/n$ and both Saxell et al. and Park et al. indicated space group *C*2/*c* instead.

The DSC results, taken together with the TGA, PXRD and SCXRD results, indicated that PM-5 (cf. CM-I or F-II) is the metastable form and converts via a solid–solid phase transition into the higher melting, thermodynamically stable polymorph PM-1 (cf. CM-V or F-I) at temperatures well below its melting point of *ca.* 195 °C. The latter (PM-1) melts at *ca*. 206 °C and the enthalpy of melting is about 100 J $g^{-1}$. These observations explain the appearance of two melting endotherms in the DSC and the disappearance of the endotherm at lower temperatures when the heating rate is very slow, e.g. 1 °C $min^{-1}$. It also explains why heat treatment at 150 °C, of the sample prepared by recrystallization from acetonitrile, produced a near-pure polymorph CM-1.

The crystal structures determined for the solvates PM-2, PM-3 and PM-4 showed a degree of similarity in terms of the packing of the molecules. However, the structures PM-1 and PM-5 were significantly different from each other, and from the rest of the structures. Of interest is the fact that, despite the structural differences, the same basic hydrogen bonding motif is present in all the structures. This explains why the melting enthalpies of the two forms are nearly the same and why it was difficult to determine the solid–solid phase transition temperature in DSC studies.

**Acknowledgements** This work is supported in part by Department of Higher Education and Training (DHET, South Africa) under the USDP funding instrument. The findings and opinions are that of the author and DHET accepts no liability. Part of this work was funded by the Deutsche Forschungsgemeinschaft (DFG) [Grant AN 212/22-2]. The authors express their gratitude to Avima (Pty) Ltd, South Africa, for the donation of the fipronil sample.

**Author Contributions** All authors contributed to the study conception and design. Material preparation and data collection were performed by DSM and ABM. All authors contributed to the data analysis. The first draft of the manuscript was written by DSM and all authors commented on previous versions of the manuscript. All authors read and approved the final manuscript.

**Funding** Open access funding provided by University of Pretoria.

## Declarations

**Conflict of interest** The authors declare that they have no competing financial interests or personal relationships that could have appeared to influence the work reported in this paper.



## References

1. Threlfall TL. Analysis of organic polymorphs. A Rev Anal. 1995;120(10):2435–60. https://doi.org/10.1039/AN9952002435.
2. Chapman D. The polymorphism of glycerides. Chem Rev. 1962;62(5):433–56.
3. Bernstein J. Polymorphism in Molecular Crystals 2e. International Union of Crystal; 2020.
4. Bhatia A, Chopra S, Nagpal K, Deb PK, Tekade M, Tekade RK. Chapter 2 - Polymorphism and its Implications in Pharmaceutical Product Development. In: Tekade RK, editor. Dosage Form Design Parameters. Academic Press; 2018. p. 31–65.
5. Roy S, Aitipamula S, Nangia A. Thermochemical analysis of venlafaxine hydrochloride polymorphs 1–5. Cryst Growth Des. 2005;5(6):2268–76.
6. Zamir S, inventor Adama Makhteshim Ltd., assignee. Polymorphs and amorphous forms of 5-amino-1[2,6-dichloro-4-(trifluoromethyl)phenyl]-4-[(trifluoromethyl)sulfinyl]-1H-pyrazole-carbonitrile, US 9,215,873 B22015.
7. Saxell HE, Erk P, Taranta C, Kröhl T, Cox G, Sukopp M et al., inventors; BASF SE, Ludwigshafen (DE), assignee. Crystalline modification of fipronil, US 8,913,473 B22018.
8. Gols R, WallisDeVries MF, van Loon JJ. Reprotoxic effects of the systemic insecticide fipronil on the butterfly Pieris brassicae. Proc R Soc B. 1922;2020(287):20192665.
9. Tingle CC, Rother JA, Dewhurst CF, Lauer S, King WJ. Fipronil: environmental fate, ecotoxicology, and human health concerns. Reviews of environmental contamination and toxicology. Springer; 2003. p. 1–66.
10. Gupta RC, Anadón A. Fipronil. Veterinary Toxicology. Elsevier; 2018. p. 533–8.
11. Simon-Delso N, Amaral-Rogers V, Belzunces LP, Bonmatin JM, Chagnon M, Downs C, et al. Systemic insecticides (neonicotinoids and fipronil): trends, uses, mode of action and metabolites. Environ Sci Pollut Res. 2015;22(1):5–34. https://doi.org/10.1007/s11356-014-3470-y.
12. Jackson D, Cornell C, Luukinen B, Buhl K, Stone D. Fipronil technical fact sheet. National Pesticide Information Center: Oregon State University Extension Services; 2009.
13. Moraes B, Menezes C, Leitemperger J, do Amaral AMB, Loro VL, Clasen B,. Comparative study on diet added with organic and inorganic selenium forms provided to carps exposed to fipronil insecticide. Water Air Soil Pollut. 2020;231(3):1–12.

14. Margarido TCS, Felício AA, de Cerqueira R-F, de Almeida EA. Biochemical biomarkers in Scinax fuscovarius tadpoles exposed to a commercial formulation of the pesticide fipronil. Mar Environ Res. 2013;91:61–7.
15. Kumar N, Kumar R, Shakil NA, Sarkar DJ, Chander S. Evaluation of fipronil nanoformulations for effective management of brown plant hopper (Nilaparvata lugens) in rice. Int J Pest Manage. 2019;65(1):86–93.
16. Saxell HE, Erk P, Taranta C, Kröhl T, Cox G, Desiraju GR et al., inventors; BASF SE, Ludwigshafen (DE), assignee. Crystalline modification of fipronil, US 8,791,046 B22014.
17. Saxell HE, Erk P, Taranta C, Kröhl T, Cox G, Sukopp M et al., inventors; BASF SE, assignee. Crystalline modification of fipronil, US 8,383,664 B22013.
18. Saxell HE, Erk P, Taranta C, Kröhl T, Cox G, Desiraju GR et al., inventors; BASF SE, Ludwigshafen (DE), assignee. Crystalline modification of fipronil, US 8,063,092 B22011.
19. Zamir S, inventor Makhteshim Chemical Works Ltd., assignee. Polymorphs and amorphous forms of 5-amino-1[2,6-dichloro-4-(trifluoromethyl)phenyl]-4-[(trifluoromethyl)sulfinyl]-1H-pyrazole-carbonitrile, US 8,440,709 B22013.
20. Park H, Kim J, Kwon E, Kim TH. Crystal structure of fipronil. Acta Crystall Sect E: Crystallogr Commun. 2017;73(10):1472–4.
21. Tang R-Y, Zhong P, Lin Q-L, Hu M-L, Shi Q. 5-Amino-1-[2,6-dichloro-4-(trifluoromethyl)phenyl]-4-(trifluoromethylsulfanyl)-1H-pyrazole-3-carbonitrile. Acta Crystallogr Sect E. 2005;61(12):4374–5.
22. Rigaku O, CrysAlis PRO. Software system. Oxford, UK: Rigaku Corporation; 2018.
23. Sheldrick GM. SHELXT–Integrated space-group and crystal-structure determination. Acta Crystallogr Sect A: Foundat Adv. 2015;71(1):3–8.
24. Farrugia LJ. WinGX and ORTEP for Windows: an update. J Appl Crystallogr. 2012;45(4):849–54.
25. Sheldrick GM. Crystal structure refinement with SHELXL. Acta Crystallogr Sect C: Struct Chem. 2015;71(1):3–8.
26. Macrae CF, Edgington PR, McCabe P, Pidcock E, Shields GP, Taylor R, et al. Mercury: visualization and analysis of crystal structures. J Appl Crystallogr. 2006;39(3):453–7.
27. Spek AL. PLATON SQUEEZE: a tool for the calculation of the disordered solvent contribution to the calculated structure factors. Acta Crystallogr Sect C: Structural Chem. 2015;71(1):9–18.
28. Moyo DS, Mapossa AB, Rademeyer M, van der Merwe EM, Focke WW. TGA investigation of the volatilisation of fipronil at elevated temperatures. Thermochim Acta. 2022. https://doi.org/10.1016/j.tca.2022.179379.
29. Hilfiker R. Polymorphism: in the Pharmaceutical Industry. Weinheim: Wiley-VCH Verlag GmbH & Co. KGaA; 2006.
30. Stephenson W. M. Kuhnert-Brandstätter, Thermomicroscopy in the analysis of pharmaceuticals: International Series of Monographs in Analytical Chemistry, Vol. 45, Pergamon Press, Oxford, 1971, 409 pp.: Elsevier; 1973.
31. Groom CR, Allen FH. The Cambridge Structural Database in retrospect and prospect. Angew Chem Int Ed. 2014;53(3):662–71.